Structural Energetics and Base-Pair Opening Dynamics in Sarcin−Ricin Domain RNA

Congju Chen,[‡] Lihong Jiang,[‡,§] Ryszard Michalczyk,[||] and Irina M. Russu*[,‡]

Department of Chemistry and Molecular Biophysics Program, Wesleyan University, Middletown, Connecticut 06459, and Bioscience Division, Los Alamos National Laboratory, Los Alamos, New Mexico 87545

Received May 8, 2006; Revised Manuscript Received August 22, 2006

ABSTRACT: The sarcin−ricin domain is a universal element of the RNA from the large ribosomal subunit. The domain is part of the binding site for elongation factors and is specifically cleaved by the toxins α-sarcin and ricin. In this work, we have mapped the energetics and dynamics of individual structural motifs in a 29-mer RNA oligomer containing the sarcin−ricin domain. The stability of individual base pairs in the structure was characterized from measurements of the exchange rates of imino protons using nuclear magnetic resonance spectroscopy at 10 °C. The measurements also provided the rates of opening and closing for selected base pairs. The results reveal that the structural stabilization free energies in the sarcin−ricin domain are broadly distributed between 2.9 and 10.6 kcal/mol. One of the least stable sites in the structure is the noncanonical G-A base pair located next to the phosphodiester bond that is cleaved by α-sarcin. The low stability of this base pair supports the proposal that cleavage by α-sarcin occurs by a base flipping mechanism. The opening dynamics of other base pairs is affected by elements of the structure such as the bulged-G motif and its cross-strand stacking. Participation in these motifs increases the lifetimes of the bases in an open, solvent-accessible conformation.

The sarcin−ricin domain (SRD)[1] is an element of the large subunit ribosomal RNA that is essential for binding of elongation factors to the ribosome and for initiation of protein synthesis. The RNA includes the 12-nucleotide sequence 5′-AGUACGAGAGGA-3′ that is highly conserved in the ribosomes from all three kingdoms of life. The domain is named for α-sarcin and ricin, two ribotoxins that catalyze the cleavage of specific bonds in the RNA. One toxin, α-sarcin, cleaves the phosphodiester bond between the eighth and ninth nucleotides in the conserved sequence (*1*); the other toxin, ricin, depurinates the adenine in the seventh position in the conserved sequence (*2*). Both processes are lethal for cells because, when SRD is modified by either toxin, the binding of elongation factors to the ribosome is impaired such that protein synthesis stops.

The structure of a 29-mer RNA oligoribonucleotide containing the SRD sequence from mammalian (rat) 28S ribosomal RNA has been determined by NMR spectroscopy (*3*, *4*) and by crystallography (*5*). The oligonucleotide is a substrate for α-sarcin (*6*). The NMR solution structure is shown in Figure 1A, and the main elements of the structure are presented schematically in Figure 1B. The first six bases and the last six bases (G_1-C_6 and $G_{24}-C_{29}$, respectively) form a double-helical stem with canonical Watson−Crick base pairs. The stem is connected to the rest of the structure by a flexible region that consists of two pyrimidine-

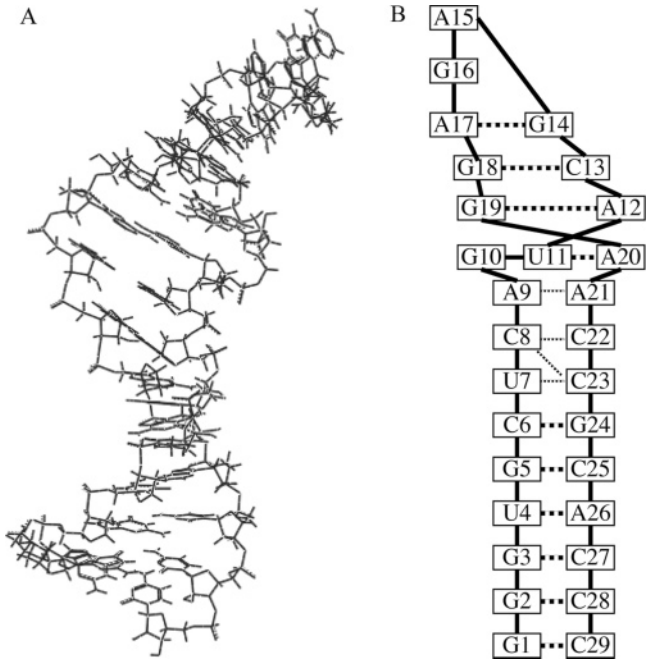

FIGURE 1: (A) NMR structure of eukaryotic (rat) SRD RNA (PDB entry 1SCL). (B) Schematic diagram of SRD RNA. The interrupted lines represent base pairing hydrogen bonding; the dotted lines represent interbase hydrogen bonds proposed on the basis of the crystallographic structure (*5*). The position of boxes approximates the base stacks observed in the structure, e.g., $G_{10}-G_{19}-G_{18}$, $A_{12}-A_{20}$, and $A_{17}-G_{16}-A_{15}$.

* To whom correpondence should be addressed. Phone: (860) 685-2428. Fax: (860) 685-2211. E-mail: irussu@wesleyan.edu.

[‡] Wesleyan University.

[§] Present address: Department of Diagnostic Radiology, Yale University School of Medicine, 300 Cedar St., New Haven, CT 06510.

[||] Los Alamos National Laboratory.

[1] Abbreviations: SRD, sarcin−ricin domain; GNRA tetraloop, loop of four nucleotides with a guanine-any nucleotide-purine-adenine sequence; NTP, nucleotide triphosphate; GTP, guanosine triphosphate; GMP, guanosine monophosphate; EDTA, ethylenediaminetetraacetic acid; HSQC, heteronuclear single-quantum coherence spectroscopy; fHSQC, fast HSQC.

10.1021/bi060908n CCC: $33.50
Published on Web 10/24/2006

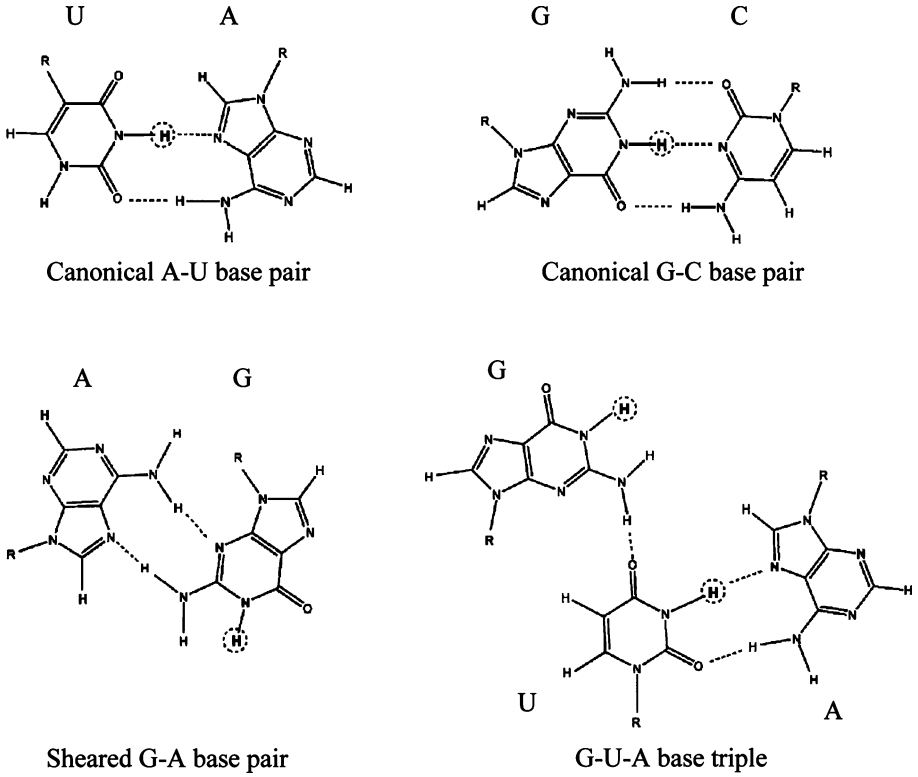

FIGURE 2: Modes of base pairing present in the SRD RNA structure. The imino protons are represented by dashed circles.

pyrimidine pairs (U_7···C_{23} and C_8···C_{22}) and the A_9···A_{21} pair. The conserved 12-nucleotide sequence encompasses positions 9−20 and folds into two structural motifs: a GAGA tetraloop and a bulged-G motif. A canonical G-C base pair (G_{18}-C_{13}) provides the junction between the two motifs. The GAGA tetraloop (G_{14}−A_{17}) belongs to the family of GNRA tetraloops (N is any nucleotide and R is purine). Like in all GNRA tetraloops (*7*), the first guanine (G_{14}) forms a sheared base pair with the last adenine (A_{17}). The GAGA tetraloop contains the sites of action for ricin (A_{15}) and α-sarcin (G_{16}-p-A_{17}). The bulged-G motif takes its name from the bulged guanine, G_{10}. This base participates in a base triple with the U_{11}-A_{20} reversed Hoogsteen pair (Figure 2) and, due to its bulged position, induces a sharp kink in the helix. The bulged G_{10} is critical for recognition of SRD RNA by α-sarcin (*8*). Other signatures of the bulged-G motif are the cross-strand stacks between A_{12} and A_{20} and between G_{10} and G_{19}.

Determination of the SRD structure has represented an important step in unraveling the rules that govern RNA folding. In spite of its relatively small size, the structure is modular in nature and forms via the assembly of well-defined, smaller motifs. Furthermore, the structure is rich in noncanonical base pairs, which could not have been predicted by the base sequence alone. This high level of compact organization raises the question of how, and how much, individual base pairs and structural modules contribute to the stability of the final structure. Equally important is the question of how the local flexibility of base pairs or structural motifs contributes to the recognition of this RNA by the two toxins. This work addresses these questions using proton exchange and nuclear magnetic resonance (NMR) spectroscopy. The concurrent use of these two techniques allows observation of individual bases in the RNA and quantitative evaluation of the stabilization free energy of a given structural element.

EXPERIMENTAL PROCEDURES

Materials

The SRD 29-mer RNA was synthesized by in vitro transcription using T7 RNA polymerase (*9*). The reaction mixture contained 40 mM Tris, 5 mM dithiothreitol, 1 mM spermidine, 0.01% Triton X-100, 20 mM $MgCl_2$, 4 mM NTPs, 250 nM DNA template, and 250 nM T7 RNA polymerase at pH 8.0. The reaction was conducted at 37 °C for 4 h and was quenched by adding EDTA to a final concentration of 50 mM. [^{15}N]GTP was either purchased from Spectra Stable Isotopes (Columbia, MD) or synthesized through phosphorylation of [^{15}N]GMP. The RNA was extracted by using a phenol/chloroform/isoamyl mixture (25:24:1 volume ratio) followed by a chloroform/isoamyl mixture (24:1 volume ratio) and then precipitated with cold 70% ethanol. The RNA was purified on a 15% sequencing gel. The final NMR samples contained 1−2 mM RNA in 10 mM phosphate buffer with 50 mM KCl, 15 mM NaCl, and 0.5 mM EDTA in 90% H_2O/10% D_2O mixture at pH 8.3 ± 0.1 (at 10 °C). These solvent conditions are the same as those previously used in the NMR structure determination (*3*). For the measurements of the exchange rates of G_{10} and G_{14} imino protons, 0.7 mM $MgCl_2$ was added to the RNA sample (in the absence of EDTA) to resolve their resonances (Results). All NMR samples also contained 0.5 mM triethanolamine, which was used to determine the pH of the samples directly in the NMR tube as we have described previously (*10*).

Methods

NMR Experiments. The NMR experiments were carried out at 10 °C on a Varian INOVA 500 spectrometer operating at 11.75 T. The exchange rates of RNA imino protons were measured by transfer of magnetization from water. The water

proton resonance was selectively inverted using a Gaussian 180° pulse (5.8 ms) followed by a variable delay for the exchange of magnetization between water and imino protons. A gradient of 0.21 G/cm was applied during the exchange delay to prevent the effects of radiation damping upon the recovery of water magnetization to equilibrium. Twenty-five values of the exchange delay in the range from 1 to 800 ms were used in each experiment. The exchange rates were calculated from the dependence of the intensity of the imino proton resonance on the exchange delay as described previously (*11*). For the unlabeled RNA samples, spectra were obtained with the jump-and-return pulse sequence (*12*). For the ^{15}N-labeled sample, spectra were obtained with the one-dimensional (1D) version of the fast HSQC (fHSQC) pulse sequence (*13*) to edit the resonances of protons attached to ^{15}N. A modified fHSQC pulse sequence (*14*) was used to eliminate the resonances of protons attached to ^{15}N and retain all other proton resonances. The highest exchange rates that could be measured by these methods are 60−70 s^{-1}. For three imino protons of SRD RNA (namely, U_7, G_{10}, and G_{14}) the exchange rates in the presence of ammonia are faster than 60−70 s^{-1}. For these protons, the exchange rates (k_{ex}) were calculated from the line width of the resonance at half-height ($\Delta\nu_{1/2}$) at a given ammonia concentration according to the equation (*15*)

$$k_{ex} = \pi\Delta\nu_{1/2} - 1/T_2 \quad (1)$$

The transverse relaxation rate, $1/T_2$, was obtained from the resonance line width in the absence of ammonia. Under these conditions, the exchange rates of the imino protons are small and can be measured by transfer of magnetization from water.

Imino Proton Exchange in RNA. The exchange of imino protons in nucleic acids is a two-step process. In the first step, the base flips out of the structure into an open state in which the barriers to exchange are removed. In the open state, the imino proton is accessible to proton acceptors, and any hydrogen bond(s) in which the proton participates breaks. The second step is the actual transfer of the proton to an acceptor such as OH^- or NH_3. The exchange rate observed experimentally is given as (*16*)

$$k_{ex} = \frac{k_{op}k_{ex,open}}{k_{cl} + k_{ex,open}} \quad (2)$$

where k_{op} and k_{cl} are the rates of opening and closing, respectively, of the base containing the imino proton and $k_{ex,open}$ is the rate of exchange from the open state. The rates of opening and closing are related to the lifetimes of the base in the closed, paired state and in the open, solvent-accessible state (τ_{cl} and τ_{op}, respectively) as

$$\tau_{cl} = \frac{1}{k_{op}} \text{ and } \tau_{op} = \frac{1}{k_{cl}} \quad (3)$$

The rate of exchange from the open state depends on the concentration of proton acceptor B as

$$k_{ex,open} = \alpha k_B[B] \quad (4)$$

where k_B is the rate constant for the transfer of the imino proton in isolated nucleotides and α is a factor that accounts for differences in the proton transfer rate between isolated nucleotides and open base pairs.

Two kinetic regimes for imino proton exchange can be distinguished depending on how the rate of exchange from the open state compares with the rate of closing. When the concentration of the proton acceptor is sufficiently high to make the exchange from the open state very fast [$k_{ex,open} \gg k_{cl}$ (EX1 regime)], the exchange is limited by the rate of base opening. In this case, eq 2 becomes

$$k_{ex} = k_{op} \quad (5)$$

At low concentrations of proton acceptor, $k_{ex,open} \ll k_{cl}$ (EX2 regime). In this regime, the observed exchange rate is proportional to the concentration of proton acceptor:

$$k_{ex} = K_{op}k_{ex,open} = K_{op}\alpha k_B[B] \quad (6)$$

where K_{op} ($=k_{op}/k_{cl}$) is the equilibrium constant for opening of the base. This equilibrium constant is related to the free energy change in the opening reaction by

$$\Delta G_{op} = -RT \ln K_{op} \quad (7)$$

where T is the absolute temperature and R is the universal gas constant.

In this work, we have used ammonia base (NH_3) as the imino proton acceptor in the exchange. Previous work from this and other laboratories has shown that, due to its small size and its lack of charge, ammonia base is the acceptor of choice for proton exchange studies of nucleic acids (*11*, *17*). The rate constant for the transfer of protons to NH_3 was calculated according to the analysis of Benight and co-workers (*18*) as 8.8×10^8 M^{-1} s^{-1} for both guanine and uracil at 10 °C. The factor α (eq 4) was assumed to have a value of 1 (*19*). The concentration of ammonia base NH_3 was calculated from the total ammonia concentration (C_0) and the pH as

$$[B] = C_0 \times 10^{-pK}/(10^{-pH} + 10^{-pK}) \quad (8)$$

The pH was measured at each ammonia concentration, directly in the NMR tube, using the proton resonances of triethanolamine (*10*). The pK value of ammonia at 10 °C is 9.73 (*20*).

RESULTS

The NMR resonances of imino protons in SRD RNA (namely, N_1H from guanines and N_3H from uracils) are shown in Figure 3A. As one can see, except for one, all expected imino proton resonances are observed. The missing resonance is that of N_1H of the second guanine in the GAGA tetraloop (G_{16}). The fact that this resonance is not observed indicates that N_1H of G_{16} exchanges very fast with water protons (k_{ex} greater than $\sim 3 \times 10^4$ s^{-1}). Of the observed imino proton resonances, most are well-resolved. The exceptions are the resonances of G_{18} and U_{11} imino protons and the resonances of G_{10} and G_{14} imino protons. To separate the resonances of G_{18} and U_{11}, we have synthesized a SRD RNA molecule containing ^{15}N-labeled guanine. The imino proton resonances of guanines were edited using 1D fHSQC, and the result is shown in Figure 3B. To edit the imino proton resonance of U_{11}, we took advantage of the fact that the

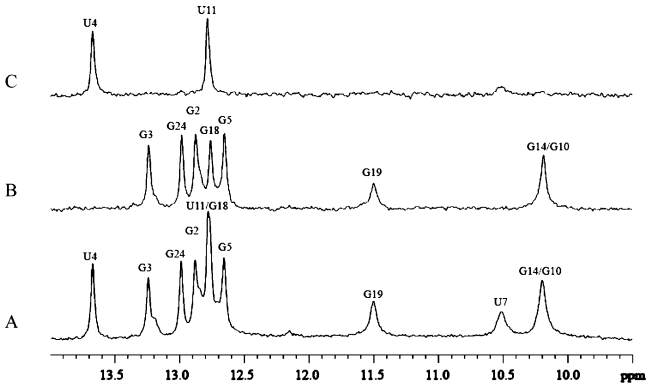

FIGURE 3: NMR resonances of imino protons in the SRD RNA. (A) All imino proton resonances in the unlabeled sample. The assignments of resonances to individual imino protons were previously published by Moore and co-workers (*3*, *29*). (B) Resonances of guanine imino protons in SRD RNA specifically labeled with ^{15}N at guanines. (C) Resonances of uracil imino protons in SRD RNA specifically labeled with ^{15}N at guanines.

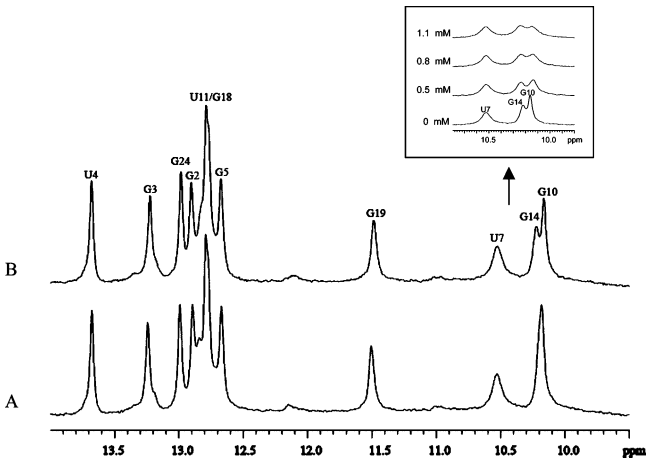

FIGURE 4: Comparison of the imino proton resonances of SRD RNA in the absence (A) and in the presence (B) of 0.7 mM Mg^{2+} ions. The inset shows the U_7, G_{14}, and G_{10} imino proton resonances in the presence of 0.7 mM Mg^{2+} ions at increasing concentrations of ammonia.

spectral region from ~10 to ~14 ppm contains only imino proton resonances from guanines and uracils. Thus, the resonances of uracils were edited using the same sample with ^{15}N-labeled guanines and a modified fHSQC pulse sequence that selects the resonances of ^{14}N-bound protons and eliminates the resonances of ^{15}N-bound protons. The result is shown in Figure 3C.

For G_{10} and G_{14}, we were unable to resolve their imino proton resonances by two-dimensional HSQC. This is because, like the ^{1}H chemical shifts, the ^{15}N chemical shifts of the imino groups of these bases are also degenerate, and the corresponding HSQC cross-peaks overlap (results not shown and ref *3*). An alternative way to separate the G_{10} and G_{14} imino proton resonances was suggested by the observation that low concentrations of Mg^{2+} ions shift the G_{10} and G_{14} imino proton resonances in opposite directions. In the presence of 0.7 mM Mg^{2+}, the two resonances are resolved from each other (Figure 4B). We have used this effect to measure the exchange rates of the two protons separately, using the line width of the two resonances as illustrated in the inset of Figure 4.

To characterize the opening reactions of individual base pairs in SRD RNA, we measured the exchange rates of imino

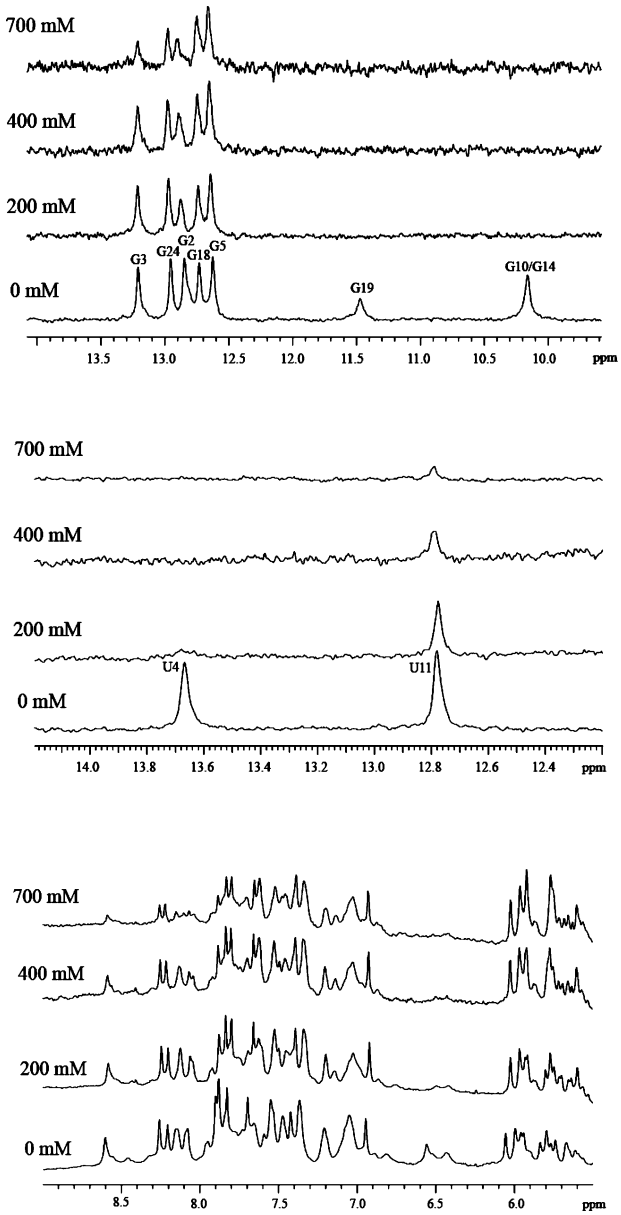

FIGURE 5: Selected regions of the ^{1}H NMR spectra of ^{15}N-labeled SRD RNA at various ammonia concentrations, in 10 mM phosphate buffer with 50 mM KCl, 15 mM NaCl, and 0.5 mM EDTA (pH 8.3).

protons as a function of ammonia concentration. The NMR spectra indicate that the RNA conformation is maintained at increasing ammonia concentrations. This result is illustrated in Figure 5 by the resonances of imino and aromatic protons. Over the range of ammonia concentrations that was investigated (i.e., 0−700 mM), there are no chemical shift changes for imino protons. Changes in chemical shift are observed for some resonances in the aromatic region, but all are less than 0.1 ppm (for example, the H2 proton resonance of A_{20} shifts from 7.88 to 7.83 ppm when the ammonia concentration increases from 0 to 700 mM). No significant changes in the line width of nonexchangeable proton resonances are observed. These findings indicate that ammonia does not significantly affect the conformation of the SRD RNA molecule. Representative examples of the dependence of exchange rates on the concentration of ammonia base are shown in Figure 6. As one can see, for the imino proton of U_{11}, the exchange rate reaches the EX1

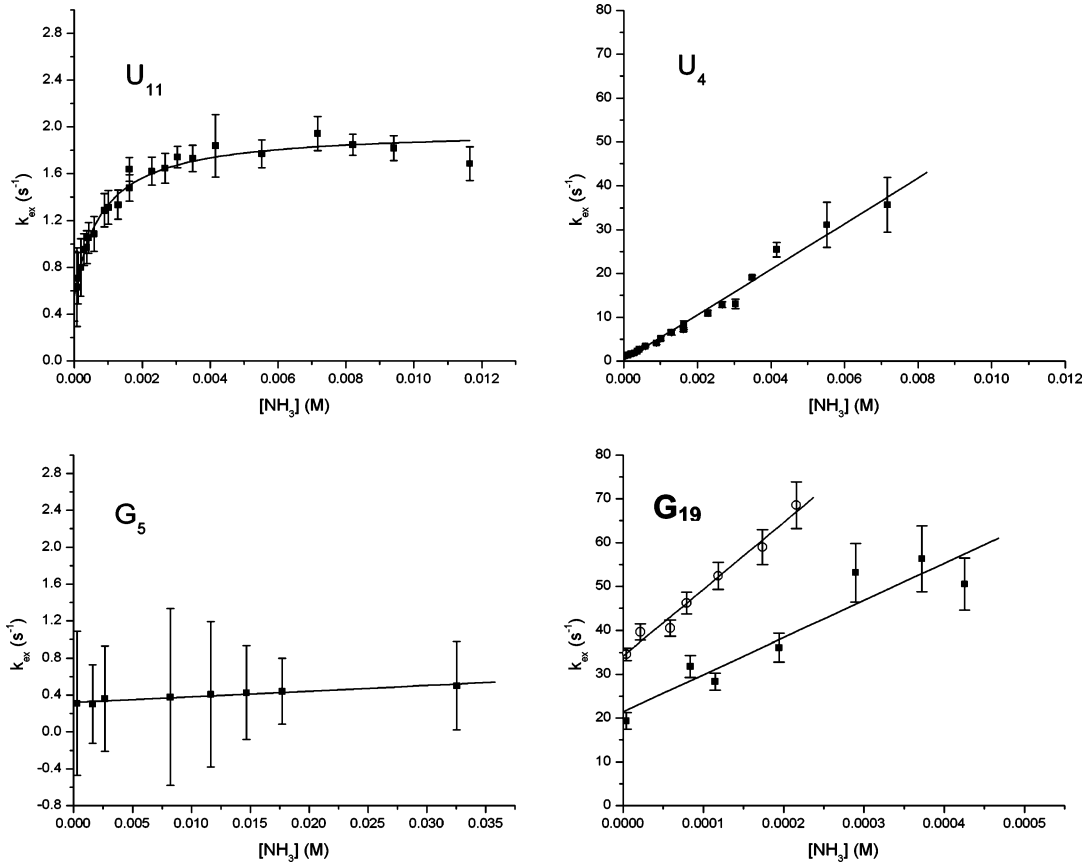

FIGURE 6: Representative examples of the dependence of the imino proton exchange rates in SRD RNA on the concentration of ammonia base, in 10 mM phosphate buffer with 50 mM KCl, 15 mM NaCl, and 0.5 mM EDTA (pH 8.3). For U_{11}, the curve represents a nonlinear least-squares fit to eq 2. For the other three imino protons, the lines represent linear fits to eq 6. For G_{19}, the empty symbols represent exchange rates in the presence of 0.7 mM Mg^{2+} ions.

regime, as predicted by eq 2. For the imino proton of G_5, the exchange rate has only a weak dependence on the concentration of ammonia base. As we show below, this finding reflects the small equilibrium constant for opening the G_5-C_{25} base pair. For G_{19} and U_4 imino protons, the exchange rates are fast even at low ammonia concentrations. With an increase in the ammonia concentration, the exchange rates further increase and become too fast for measurement by transfer of magnetization from water. Hence, for these protons, only data in the EX2 regime could be obtained. One notes also that, in the absence of added ammonia, the exchange rate of the G_{19} imino proton is $\sim$20 s^{-1} (or $\sim$35 s^{-1} in the presence of Mg^{2+} ions), whereas for all the other protons shown, the exchange rates are close to zero. These differences are due to the catalysis of the exchange by OH^- ions present in solution at pH 8.3. The OH^- catalysis does not make a significant contribution to the observed exchange rate when the opening equilibrium constant (K_{op}) is small (eq 6). This is the case for U_{11}, U_4, and G_5. In contrast, for G_{19}, the K_{op} value is much larger (vide infra) and OH^- catalysis yields a high exchange rate even in the absence of added ammonia. The presence of 0.7 mM Mg^{2+} ions affects the exchange rates of two imino protons: the exchange rate of the G_{19} imino proton is increased (Figure 6) and that of the U_7 imino proton decreased. For all the other imino protons, the exchange rates in the presence of 0.7 mM Mg^{2+} are, within experimental error, the same as those in the absence of the ions.

Table 1: Base-Pair Opening Parameters in SRD RNA at 10 °C, in 10 mM Phosphate Buffer with 50 mM KCl, 15 mM NaCl, and 0.5 mM EDTA

imino proton	k_{op} (s^{-1})	k_{cl} ($\times 10^{-6}$ s^{-1})	K_{op} ($\times 10^6$)	ΔG_{op} (kcal/mol, at 10 °C)
G_2	15.8 ± 0.7	2.4 ± 0.4	6.5 ± 1.1	6.72 ± 0.09
G_3	2.00 ± 0.08	4.3 ± 0.8	0.47 ± 0.09	8.2 ± 0.1
U_4	*b*	*b*	5.9 ± 0.2	6.78 ± 0.02
G_5	*c*	*c*	0.0070 ± 0.0008	10.57 ± 0.06
G_{24}	*c*	*c*	0.024 ± 0.002	9.87 ± 0.05
U_7[a]	*b*	*b*	993 ± 18	3.89 ± 0.01
			697 ± 44[d]	4.09 ± 0.03[d]
G_{10}[a]	*b*	*b*	6250 ± 800[d]	2.86 ± 0.07[d]
U_{11}	1.97 ± 0.04	0.5 ± 0.1	3.8 ± 0.9	7.0 ± 0.1
G_{14}[a]	*b*	*b*	3818 ± 80[d]	3.13 ± 0.01[d]
G_{18}	3.15 ± 0.08	0.5 ± 0.1	6.3 ± 1.3	6.7 ± 0.1
G_{19}	*b*	*b*	96 ± 15	5.21 ± 0.09
			163 ± 15[d]	4.91 ± 0.09[d]

[a] From the line width measurement. [b] The exchange rates in the EX1 regime are too fast to be measured by NMR. [c] The EX1 regime could not be reached at the highest ammonia concentrations that were investigated. [d] With 0.7 mM Mg and no EDTA.

The rates k_{op} and the equilibrium constants K_{op} for base-pair opening, obtained from the dependence of the exchange rates on ammonia concentration, are summarized in Table 1. The rates of opening were obtained for only the bases in which the imino proton exchange reached the EX1 regime over the range of ammonia concentrations investigated, namely, G_2, G_3, G_{18}, and U_{11}. For the other bases, the exchange rates in the EX1 regime were too fast to be

measured by NMR (U_4, U_7, G_{10}, G_{14}, and G_{19}) or the exchange did not reach the EX1 regime at the highest concentrations of ammonia that were used (G_5 and G_{24}). In these cases, only the equilibrium constants of the opening reactions could be obtained (Table 1). The free energy change in the opening reaction, $\Delta \boldsymbol{G}_{op}$, was calculated from the opening equilibrium constant according to eq 7 (Table 1).

DISCUSSION

The proton exchange results obtained in this work allow us to define the local stabilities at different sites within the SRD RNA structure. With this approach, the structural stability at a given site is measured by the free energy change in the opening reaction, ΔG_{op}. Sites with high structural stability are characterized by low values of the equilibrium constant (K_{op}) and large values of the free energy change (ΔG_{op}). Alternatively, high K_{op} and small G_{op} values reflect low structural stabilities at the corresponding sites. Inspection of the results shown in Table 1 reveals that the opening equilibrium constants (K_{op}) in SRD RNA span 6 orders of magnitude, from 7×10^{-9} for the G_5-C_{25} base pair in the double-helical stem to 6×10^{-3} for the bulged G_{10}. This wide range of values reflects a broad distribution of structural stabilization free energies from 2.9 to 10.6 kcal/mol.

The least stable sites of SRD RNA that we observed include the two G-A base pairs (G_{14}-A_{17} and G_{19}-A_{12}) and the bulged G_{10}. The equilibrium constants (K_{op}) measured for G_{10}, G_{14}, and G_{19} are in the range from 10^{-4} to 6×10^{-3}, which is much higher than the range of K_{op} values for the double-helical part of the structure (7×10^{-9} to 6×10^{-6}). The large K_{op} values of G_{10}, G_{14}, and G_{19} are most likely due to the nature of the opening reactions for these guanines. In double-helical RNA, to bring the imino proton into a solvent-accessible state, the base must rotate away from the helix center by $\geq 50°$ (*21*, *22*). In this transition to the open state, the base overcomes the stacking interactions with its two neighboring base pairs and the partner base is also perturbed. Hence, the energetic cost of the opening reaction is high. For G-A base pairs or for the bulged G_{10}, the structural changes that yield the guanine's open state are expected to be different. This is because, in these cases, the Watson−Crick edge of the guanine faces the phosphodiester backbone. This orientation places the guanine's imino and amino groups within hydrogen bonding distance of the oxygen atoms in backbone phosphate groups (*3*, *5*). According to the crystallographic structure, the G_{10} imino group is within hydrogen bonding distance of the G_{19}-p-A_{20} phosphate, the G_{14} imino group of the G_{16}-p-A_{17} phosphate, and the G_{19} imino group of the G_{10}-p-U_{11} phosphate. The proximity of the backbone and the hydrogen bonds to the phosphates are expected to protect the imino protons from exchange with water protons. This protection explains why G_{10}, G_{14}, and G_{19} imino protons can be observed in the NMR spectra (Figure 3). The protection also explains why the exchange of these protons is slowed 160−10000-fold relative to that in free guanine (eq 6 and Table 1). Hence, the exchange of G_{10}, G_{14}, and G_{19} protons should involve breaking the hydrogen bonds to the backbone and flipping out the guanine into a fully accessible state. Our results show that the energetic cost of these changes is relatively small, yet even at this low energetic cost, the influence of stacking interactions upon opening energetics can be detected for the G_{19}-A_{12} base pair. The equilibrium constant for opening the G_{19}-A_{12} base pair is ~23-fold smaller than that for opening of the other G-A base pair, G_{14}-A_{17}. This decrease in K_{op} corresponds to an increase in the free energy of opening of G_{19} relative to G_{14} by ~1.8 kcal/mol. In the structure (Figure 1B), G_{19} stacks on G_{18} and, in the cross-strand stack, on G_{10}. These double stacking interactions should clearly increase the stability of G_{19}, as we observed. An additional factor that may contribute to the differences in stability between G_{14}-A_{17} and G_{19}-A_{12} base pairs is the pattern of interbase hydrogen bonding. In the G_{19}-A_{12} base pair, the guanine forms two hydrogen bonds to the adenine as shown in Figure 2. In contrast, for the G_{14}-A_{17} base pair, the crystallographic structure suggests that the guanine forms a single bifurcated hydrogen bond from its NH_2 group to N7 and the phosphate of A_{17} (*5*). A smaller number of interbase hydrogen bonds would decrease the stability of G_{14} in the paired conformation, as we observed.

Another part of the SRD RNA structure that is of special interest is the canonical G_{18}-C_{13} base pair at the junction between the GAGA tetraloop and the bulged-G motif (Figure 1B). Our results show that the stability of this base pair is the same as that of the penultimate G_2-C_{28} base pair in the stem [$K_{op} = (6.3 \pm 1.3) \times 10^{-6}$ for G_{18}, and $K_{op} = (6.5 \pm 1.1) \times 10^{-6}$ for G_2]. In spite of this similarity, the dynamics of G_{18}-C_{13} base pair differs from that of the G_2-C_{28} base pair. The opening rate of the G_{18}-C_{13} pair (3.15 ± 0.08 s^{-1}) is ~5-fold smaller than the opening rate of the G_2-C_{28} pair (15.8 ± 0.7 s^{-1}). As expected from the K_{op} values, the rates of the closing reactions show the same trend: $(0.5 \pm 0.1) \times 10^6$ s^{-1} for G_{18} and $(2.4 \pm 0.4) \times 10^6$ s^{-1} for G_2. Therefore, the location of the canonical G_{18}-C_{13} base pair within the SRD loop slows its closing reaction relative to that for the G-C base pair in the double-helical stem. The implication of this result is that the average lifetime of G_{18} in its open state (τ_{op}, eq 3) is longer than that of the guanine in the stem.

A similar effect of the structure on the dynamics of opening−closing reactions is observed for U_{11} . U_{11} is located at the core of the bulged-G motif where it forms a base triple with G_{10} and A_{20} (Figure 2). The opening equilibrium constant for U_{11} [$(3.8 \pm 0.9) \times 10^{-6}$] is comparable to that for U_4 in the canonical U_4-A_{26} base pair [$(5.9 \pm 0.2) \times 10^{-6}$]. Hence, participation of U_{11} in the base triple of the bulged-G motif does not enhance significantly its stability relative to that of a canonical U-A base pair from the double-helical stem. The dynamics of U_{11} is, however, different. The opening rate of U_{11} is slow (1.97 ± 0.04 s^{-1}). For U_4, the opening rate could not be determined because the exchange rate of its imino proton in the EX1 regime is too fast. Nevertheless, the exchange rates that could be measured (Figure 6) indicate that the opening rate of U_4 should be greater than ~40 s^{-1}. Thus, the opening rate of U_{11} is at least 20-fold lower than that of U_4. Since the opening equilibrium constants of the two bases are comparable, the closing rate of U_{11} should also be at least 20-fold slower than that of U_4. Hence, like for G_{18}, participation of U_{11} in the SRD structure lowers the rate of closing of this base. As a result, the average lifetime of U_{11} in the open state ($\tau_{op} = 2$ μs) is at least 20-fold longer than that in the canonical U-A base pair.

In our analysis of the dynamics and structural stability in the SRD loop discussed above, we have compared the

opening parameters of individual base pairs to those in the double-helical stem. One should note however that, within the stem, there is an appreciable variation in the opening equilibrium constants (Table 1). These variations most likely reflect the influence of the sequence context for each base pair, as observed previously for various RNA and DNA double helices (*23*−*25*). Furthermore, in the case of SRD RNA, the results suggest that the rest of the structure also influences base-pair opening in the stem. The largest effects are observed for the G-C base pairs next to the connector region, i.e., G_5-C_{25} and C_6-G_{24}. The opening equilibrium constants for these base pairs are the lowest in the SRD RNA structure and are 3−10-fold lower than those previously observed in RNA double helices of various base sequences, at the same temperature (*23*). This observation suggests that the loop and the connector region have a stabilizing effect on the upper part of the double-helical stem.

The dynamics of the SRD 29-mer RNA studied here has recently been investigated by Sponer and co-workers (*26*) using molecular dynamics simulations. Deviations from the crystallographic structure were observed for bases in the GAGA loop. Specifically, within 25 ns of simulation, G_{14} and A_{17} shift from their position in the structure such that the stacking between A_{17} and G_{18} is almost lost (Figure 1B). However, the other regions of the structure exhibited no significant molecular movements during the simulations. On the basis of these results, Sponer and co-workers suggested that SRD is a rigid RNA that, on the nanosecond time scale, does not experience alternative conformations (*26*). The results presented here complement this dynamic picture. They show that, on longer time scales (e.g., milliseconds or longer), SRD samples alternative conformational states in which individual bases are open and accessible. These opening conformational transitions may be important in the recognition of this RNA by toxins. At present, the molecular mechanisms by which α-sarcin and ricin recognize and cleave SRD RNA are not yet understood. Valuable insights into this question have been provided by the crystallographic structures of restrictocin (a close relative of α-sarcin) in complex with several analogues of the SRD RNA studied in this work (*27*). The structures confirm earlier biochemical and mutation results, which indicated that the bulged G_{10} and the surrounding S-turn in the phosphodiester backbone are the identity elements responsible for the specific binding of the toxin to SRD (*8*, *28*). Interestingly, these key recognition elements are located ∼11 Å from the G_{16}-p-A_{17} bond to be cleaved. Hence, in addition to selecting the bulged-G motif when binding to the RNA, the toxin must also identify the G_{16}-p-A_{17} bond for cleavage. In the crystallographic structures of the restrictocin−RNA complexes, the G_{14}-A_{17} base pair is disrupted, and G_{16} and A_{17} flip out of their stack. This observation suggested that the G_{16}-p-A_{17} bond is selected for cleavage by a base flipping mechanism that positions the nucleophile for in-line attack on the scissile bond (*27*). Our results support this suggestion. As we have shown, among all base pairs present in the loop of SRD, the G_{14}-A_{17} base pair has the lowest structural stabilization energy [i.e., 3.1 kcal/mol (Table 1)]. Hence, this base pair could be selected by the protein due to the small energetic cost involved in disrupting it. It is also interesting to note that, due to specific structural features of SRD RNA, the two base pairs that separate the G_{14}-A_{17} base pair from the recognition site at the bulged G_{10} are significantly more stable. The invariant G_{18}-C_{13} base pair, being a canonical base pair, is ∼3.6 kcal/mol more stable than the G_{14}-A_{17} base pair. The next base pair, G_{19}-A_{12}, has an additional interbase hydrogen bond and participates in the G_{19}−G_{10} and A_{12}−A_{20} cross-strand stacks. As a result, its stability is increased by ∼1.8 kcal/mol relative to that of the G_{14}-A_{17} base pair. The high stabilities of these two neighboring base pairs may enhance the energetic identity of the G_{14}-A_{17} base pair and thus allow its selection for base flipping and subsequent cleavage.

ACKNOWLEDGMENT

We thank Dr. Peter B. Moore and his research group at Yale University (New Haven, CT) for sharing with us their expertise in the NMR spectroscopy of SRD RNA. We also thank Dr. Smita Patel (University of Medicine and Dentistry of New Jersey-Robert Wood Johnson Medical School, Piscataway, NJ) for a gift of T7 RNA polymerase.

REFERENCES

1. Endo, Y., and Wool, I. G. (1982) The site of action of α-sarcin on eukaryotic ribosomes. The sequence at the α-sarcin cleavage site in 28S ribosomal ribonucleic acid, *J. Biol. Chem. 257*, 9054−9060.
2. Endo, Y., Mitsui, K., Motizuki, M., and Tsurugi, K. (1987) The mechanism of action of ricin and related toxic lectins on eukaryotic ribosomes. The site and the characteristics of the modification in 28S ribosomal RNA caused by the toxins, *J. Biol. Chem. 262*, 5908−5912.
3. Szewczak, A. A., and Moore, P. B. (1995) The Sarcin/Ricin Loop, a Modular RNA, *J. Mol. Biol. 247*, 81−98.
4. Warren, J. J., and Moore, P. B. (2001) Application of dipolar coupling data to the refinement of the solution structure of the Sarcin-Ricin loop RNA, *J. Biomol. NMR 20*, 311−323.
5. Correll, C. C., Munishkin, A., Chan, Y.-L., Ren, Z., Wool, I. G., and Steitz, T. A. (1998) Crystal structure of the ribosomal RNA domain essential for binding elongation factors, *Proc. Natl. Acad. Sci. U.S.A. 95*, 13436−13441.
6. Szewczak, A. A., Chan, Y. L., Moore, P. B., and Wool, I. G. (1991) On the conformation of the α sarcin stem-loop of 28S rRNA, *Biochimie 73*, 871−877.
7. Moore, P. B. (1999) Structural Motifs in RNA, *Annu. Rev. Biochem. 67*, 287−300.
8. Gluck, A., and Wool, I. G. (1996) Determination of the 28S Ribosomal RNA Identity Element (G4319) for α-Sarcin and the Relationship of Recognition to the Selection of the Catalytic Site, *J. Mol. Biol. 256*, 838−848.
9. Milligan, J. F., Groebe, D. R., Witherell, G. W., and Uhlenbeck, O. C. (1987) Oligoribonucleotide synthesis using T7 RNA polymerase and synthetic DNA templates, *Nucleic Acids Res. 15*, 8783−8798.
10. Chen, C., and Russu, I. M. (2004) Sequence-Dependence of the Energetics of Opening of AT Base Pairs in DNA, *Biophys. J. 87*, 1−7.
11. Russu, I. M. (2004) Probing Site-Specific Energetics in Proteins and Nucleic Acids by Hydrogen Exchange and NMR Spectroscopy, *Methods Enzymol. 379*, 152−175.
12. Plateau, P., and Gueron, M. (1982) Exchangeable proton NMR without base-line distortion, using new strong-pulse sequences, *J. Am. Chem. Soc. 104*, 7310−7311.
13. Mori, S., Abeygunawardana, C., Johnson, M. O., and van Zijl, P. C. M. (1995) Improved Sensitivity of HSQC Spectra of Exchanging Protons at Short Interscan Delays Using a New Fast HSQC (FHSQC) Detection Scheme That Avoids Water Saturation, *J. Magn. Reson., Ser. B 108*, 94−98.
14. Otting, G., and Wuthrich, K. (1990) Heteronuclear filters in two-dimensional [^{1}H, ^{1}H]-NMR spectroscopy: Combined use with isotope labelling for studies of macromolecular conformation and intermolecular interactions, *Q. Rev. Biophys. 23*, 39−96.

15. Sandstrom, J. (1982) *Dynamic NMR Spectroscopy*, Academic Press, London.
16. Englander, S. W., and Kallenbach, N. R. (1984) Hydrogen exchange and structural dynamics of proteins and nucleic acids, *Q. Rev. Biophys. 16*, 521−655.
17. Gueron, M., and Leroy, J. L. (1995) Studies of Base Pair Kinetics by NMR Measurement of Proton Exchange, *Methods Enzymol. 261*, 383−413.
18. Benight, A. S., Schurr, J. M., Flynn, P. F., Reid, B. R., and Wemmer, D. E. (1988) Melting of a Self-complementary DNA Minicircle. Comparison of Optical Melting Theory with Exchange Broadening of the Nuclear Magnetic Resonance Spectrum, *J. Mol. Biol. 200*, 377−399.
19. Gueron, M., Charretier, E., Hagerhorst, J., Kochoyan, M., Leroy, J. L., and Moraillon, A. (1990) in *Structure & Methods* (Sarma, R. H., and Sarma, M. H., Eds.) pp 113−137, Adenine Press, Guilderland, NY.
20. Weast, R. C. (1987) *CRC Handbook of Chemistry and Physics*, 67th ed., CRC Press, Boca Raton, FL.
21. Pan, Y., and MacKerell, A. D., Jr. (2003) Altered structural fluctuations in duplex RNA versus DNA: A conformational switch involving base pair opening, *Nucleic Acids Res. 31*, 7131−7140.
22. Varnai, P., Canalia, M., and Leroy, J.-L. (2004) Opening Mechanism of G•T/U Pairs in DNA and RNA Duplexes: A Combined Study of Imino Proton Exchange and Molecular Dynamics Simulation, *J. Am. Chem. Soc. 126*, 14659−14667.
23. Snoussi, K., and Leroy, J.-L. (2001) Imino Proton Exchange and Base-Pair Kinetics in RNA Duplexes, *Biochemistry 40*, 8898−8904.
24. Folta-Stogniew, E. J., and Russu, I. M. (1994) Sequence Dependence of Base-Pair Opening in a DNA Dodecamer Containing the CACA/GTGT Sequence Motif, *Biochemistry 33*, 11016−11024.
25. Coman, D., and Russu, I. M. (2005) Base Pair Opening in Three DNA-unwinding Elements, *J. Biol. Chem. 280*, 20216−20221.
26. Spackova, N., and Sponer, J. (2006) Molecular dynamics simulations of sarcin-ricin rRNA motif, *Nucleic Acids Res. 34*, 697−708.
27. Yang, X., Gerczei, T., Glover, L., and Correll, C. C. (2001) Crystal structures of restrictocin-inhibitor complexes with implications for RNA recognition and base flipping, *Nat. Struct. Biol. 8*, 968−973.
28. Wool, I. G., Correll, C. C., and Chan, Y.-L. (2000) in *The Ribosome: Structure, Function, Antibiotics and Cellular Interactions* (Garrett, R. A., Douthwaite, S. R., Liljas, A., Matheson, A. T., Moore, P. B., and Noller, H. F., Eds.) ASM Press, Washington, DC.
29. Seggerson, K., and Moore, P. B. (1998) Structure and stability of variants of the sarcin-ricin loop of 28S rRNA: NMR studies of the prokaryotic SRL and a functional mutant, *RNA 4*, 1203−1215.

BI060908N